PCCP

PAPER

View Article Online
View Journal

Cite this: DOI: 10.1039/c3cp54970d

Computational modeling of single- *versus* double-anchoring modes in di-branched organic sensitizers on TiO_2 surfaces: structural and electronic properties†

Joaquín Calbo,[a] Mariachiara Pastore,*[b] Edoardo Mosconi,[b] Enrique Ortí*[a] and Filippo De Angelis*[b]

We present a first-principles DFT investigation of the adsorption geometry on the anatase (101) surface of a prototypical di-branched organic dye based on the extended tetrathiafulvalene moiety, incorporating two anchoring cyanoacrylic acid units. Reduced model systems with one and two anchoring groups have been initially studied to investigate the vibrational frequencies related to TiO_2 dye adsorption. Our calculations confirm that the reduced systems can be used as reliable models to study the anchoring modes and that the conclusions extracted from the reduced systems can be extrapolated to the entire molecule. A series of molecular structures have been investigated to simulate the anchoring environment in monodentate- and bidentate-like adsorption modes. The comparison between the theoretical results and the available experimental data suggests a di-anchored monodentate adsorption mode as the most probable adsorption structure. Geometry optimizations of the di-branched model system adsorbed on a periodic slab of anatase (101) allowed us to compare the relative stability of different adsorption conformations and led to a di-anchored monodentate mode as the most stable adsorption structure. Furthermore, *ab initio* molecular dynamics simulations confirmed this structure as the preferred one, providing additional stabilization by effective hydrogen-bonding to surface oxygens and structure distortion from planarity. The analysis of the partial density of states for the prototypical models confirms that the doubly anchored adsorption provides improved electronic properties compared to the singly anchored structures for dye-sensitized solar cell purposes.

Received 25th November 2013,
Accepted 13th January 2014

DOI: 10.1039/c3cp54970d

www.rsc.org/pccp

1. Introduction

Dye-sensitized solar cells (DSCs) have attracted increasing attention in the last decade as promising alternatives to the traditional silicon-based photovoltaics.[1–3] In these devices, a dye-sensitizer absorbs the solar radiation and the photoexcited electron is transferred to the conduction band (CB) of a semiconductor, typically TiO_2 nanoparticles. Then, a redox mediator, commonly based on the iodide/triiodide couple, regenerates the oxidized dye thus completing the circuit.

Since the discovery of the highly efficient Ru(II)-based complexes, such as N3 and N719 dyes,[2,4] much effort has been made to synthesize new and more efficient push–pull organic dyes, due to their lower-cost synthesis, tunable optical properties and environmental friendliness.[5,6] However, few organic dyes with the standard I^-/I_3^- electrolyte show efficiencies that can directly compete with those of the most prominent Ru complexes.[7–9] Organic dyes in conjunction with monoelectronic metallorganic redox couples, such as Co(II)/Co(III) complexes, usually showing simpler kinetics and requiring less dye regeneration over-potentials, have led to efficiencies exceeding those of Ru(II)-based sensitizers.[10–14]

First-principles computer simulations have been shown to successfully provide new insights into the structural, electronic and optical properties of the hybrid dye/semiconductor interface in DSCs,[15] in particular providing crucial information on the preferred adsorption modes of the dye onto the semiconductor surface.[16,17] In previous work, some of us demonstrated that the highly efficient N719 exploits three of its four carboxylic acid anchoring groups in the linkage to the semiconductor surface.[18,19] This coordination through three carboxylic acids provides not

[a] *Instituto de Ciencia Molecular, Universidad de Valencia, 46980 Paterna, Spain. E-mail: enrique.orti@uv.es*
[b] *Computational Laboratory for Hybrid Organic Photovoltaics (CLHYO), Istituto CNR di Scienze e Tecnologie Molecolari, via Elce di Sotto 8, I-06123, Perugia, Italy. E-mail: chiara@thch.unipg.it, filippo@thch.unipg.it*

† Electronic supplementary information (ESI) available: Chemical structures of several di-branched dyes; calculated B3LYP and PBE0 IR spectra in the gas phase and in acetonitrile solution for compound **1**; calculated bond distances for the different models of **1**; PBE0 infrared frequencies of the main vibrational modes present in the dye@semiconductor system; electrostatic potential averages plots; and PDOS for **2**@TiO_2. See DOI: 10.1039/c3cp54970d

only high stability to the device, but also high open-circuit voltage (V_{OC}) and efficient electron injection. Thus, the design of new purely organic dyes bearing more than one anchoring group appears to be the next natural step.

In this perspective, several di-anchoring dyes have been very recently synthesized and characterized providing a general improvement in the photovoltaic performance compared to the single-anchoring homologues. Some examples of these novel di-branched dyes are the Zn-based porphyrin ZnPDCA dye,[20] and triarylamino-based absorbers such as KS-5,[21] DB-1 and DB-2[22] (see Scheme S1 in the ESI† for chemical structures). These dyes provided not only much higher short-circuit photocurrent densities (J_{SC}) and slightly higher V_{OC} than the single-branched homologues, but also improved and red-shifted incident photon-to-current efficiencies (IPCEs).

In the context of organic sensitizers, a number of push–pull π-extended tetrathiafulvalene (exTTF)-based systems (exTTF stands for 2-[9-(1,3-dithiol-2-ylidene)anthracen-10(9*H*)-ylidene]-1,3-dithiole) have emerged as novel promising dyes, which absorb light in a wide range of the UV-Vis and NIR spectrum.[23] This is mainly due to the improved donor ability of the exTTF unit, which produces a notable increase in the energy of the highest-occupied molecular orbital (HOMO). Encouraged by these results, two new di-anchoring dyes containing the exTTF-related donor unit 10-(1,3-dithiol-2-ylidene)anthracene[24] have been synthesized.[25] The only difference between these two novel dyes relies on the π-spacer separating the donor unit and the anchoring cyanoacrylic acid group: a simple benzene ring for **A** and the 3,4-ethylenedioxythiophene (EDOT) unit for **B** (Fig. 1). The use of EDOT spacers has been inspired by previous work, where the EDOT was shown to yield a red-shift in the spectroscopic response and an enhancement of the molar extinction coefficient in triphenylamine and exTTF-based sensitizers.[23,26,27] However, the lower performance of **B** in the device, in line with previous findings, suggests fast recombination processes as a consequence of I_2–EDOT interactions that do not occur in **A**.[28] From the FTIR spectra recorded for **A** and **B**, a di-anchoring adsorption mode on the TiO_2 surface was found on the basis of the disappearance of the stretching vibration of the carbonyl group at around 1700 cm^{-1} in passing from the powder spectra to the dye-adsorbed spectra.[25] However, the adsorption mode of each anchoring group to the semiconductor surface is much more difficult to determine.

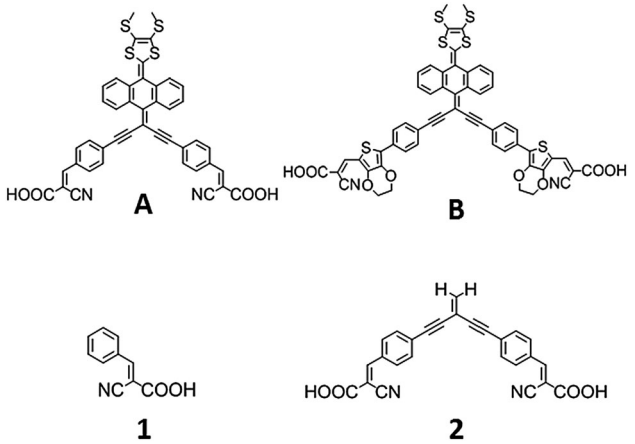

Fig. 1 Dyes **A** and **B** and the two size-reduced systems, with one (**1**) and two (**2**) anchoring groups, used as models of dye **A**.

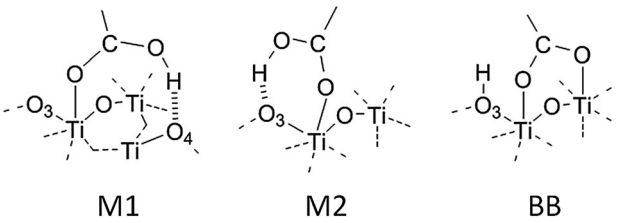

Fig. 2 Graphical representation of the three main carboxylic/carboxylate binding modes in DSCs: two different monodentate (M1 and M2) and one bridged bidentate (BB) adsorptions.

We recall that the anchoring mechanism of a carboxylic-based dye onto the TiO_2 surface can be simplified by the different coordination modes of the carboxylic acid/carboxylate unit ($COOH/COO^-$) to the metal ions.[29] Thus, it is possible to differentiate between three anchoring modes: monodentate (M), chelated (CB) and bridged bidentate (BB). Among them, the monodentate and especially the bridged bidentate modes displayed in Fig. 2 are the most common modes found in the field of organic sensitizers attached to the TiO_2 anatase (101) surface.[16,30–34] In the case of the monodentate, two binding modes, M1 and M2, are distinguishable due to the oxygen atom (O_4 or O_3, respectively) to which the carboxylic hydrogen is linked.[29] A distinction between the monodentate and bidentate modes can be obtained by means of the empirical rule derived by Deacon and Philips, which correlates the difference between the asymmetric and symmetric stretching wavenumbers ($\Delta\nu_{as}$) of COO^- to the type of coordination.[35] In broad terms, a measurement of $\Delta\nu_{as}$ close or smaller than the reference value for the neat salt (usually about 200 cm^{-1}) indicates a bridged bidentate coordination, whereas a value of $\Delta\nu_{as}$ larger than the reference value is related to a monodentate adsorption. Experimentally, the identification of the symmetric and asymmetric stretching COO^- frequencies is only feasible for simple acids, due to the overlap of new and intense bands in the 1400–1600 cm^{-1} region occurring for aromatic and conjugated systems. For the two novel di-branched sensitizers **A** and **B**, a value of $\Delta\nu_{as}$ = 220–260 cm^{-1} was preliminarily proposed thus sitting at the edge of a possible assignment.

In this contribution, we theoretically investigate the relative stabilities of the different anchoring modes for sensitizer **A**. First, a comprehensive determination of the vibrational features of the sensitizer by varying the nature of the carboxylic anchorage allows for the understanding on how the anchorage of the dye to the TiO_2 surface modifies the fundamental frequencies of the carboxylic/carboxylate group. The theoretical characterization of the typical vibrational modes in a dye@TiO_2-like system enables us to unequivocally assign the symmetric and asymmetric CO modes in the available experimental FTIR spectrum. In a second step, a reduced model system of **A** is used to compare the relative

stabilities of the different considered anchoring modes. The geometry of all the systems is carefully examined and a long *ab initio* molecular dynamics is carried out for the conformer with the most stable adsorption mode. Finally, the role of the adsorption topology in influencing the electronic properties of the system is discussed on the basis of a detailed analysis of the density-of-states profiles. To our knowledge, this study represents the first investigation of the anchoring mode for a di-branched organic dye, opening the way to a full exploitation of this class of potential highly efficient dyes.

2. Methodology

To limit the computational cost, two simpler models of dye **A** incorporating one and two cyanoacrylic acid groups (compounds **1** and **2**, respectively, in Fig. 1) were used. Density functional theory (DFT) calculations were performed at the B3LYP/6-31G* level,[36,37] in conjunction with the polarizable continuum model (PCM)[38,39] approach using acetonitrile as solvent. The vibrational frequencies obtained were corrected according to the vibrational scaling factor of 0.960 reported in the literature.[40–43] Geometry optimizations and frequency calculations for the systems under study were carried out using the Gaussian 09 program package (version C.01).[44]

To model the adsorption of the dye to the anatase (101) surface, a periodic slab of $(TiO_2)_n$ with $n = 64$ was employed, being large enough to accommodate the dye in a di-branched monodentate mode. It has been recently shown that TiO_2 anatase slabs of thickness similar to our modeled slab (two-layer fashion) nicely reproduce the electronic structure of thicker films.[45] Because of the molecular rigidity of the dye, a transversal analogue with $n = 72$ was necessary to allow a di-anchoring bridged bidentate mode. The other possible adsorption modes were modeled using the $n = 64$ slab to reduce the computational cost, still maintaining the reliability of the results. The energy difference between the $n = 64$ and $n = 72$ periodic slabs was used to rescale the absolute energy of the investigated configurations in order to compare the relative stability computed on different-sized slabs.

Periodic calculations were performed using DFT within the generalized gradient approximation (GGA) by means of the PBE exchange–correlation functional.[46] The Car–Parrinello (CP) algorithm[47] was employed as implemented in the Quantum-Espresso 5.0 package[48] for both geometry optimizations and *ab initio* dynamics simulations. Electron–ion interactions were described by ultrasoft pseudopotentials with electrons from O, N and C 2s, 2p, H 1s, and Ti 3s, 3p, 3d, 4s shells explicitly included in the calculations. Plane-wave basis set cutoffs for the smooth part of the wave functions and the augmented density were 25 and 200 Ry, respectively. The dye molecules were adsorbed only on one side of the slab and the vacuum between the top of the molecule and the adjacent upper slab was ~ 6 Å for the largest extended single-anchored conformer. Molecular dynamics simulations were carried out with an integration time step of 10 au for a total of *ca.* 3 ps. The fictitious mass used for the electronic degrees of freedom is 1000 au, and the atomic masses for the different elements were set to 5 amu. This set-up allows us to achieve a fast equilibration of the system and to speed-up the Car–Parrinello dynamics. A randomization of the atomic positions was used to increase the potential energy and raise the temperature of the system over 150 degrees. Afterwards, a Nose–Hoover thermostat was applied to increase and maintain the temperature between 300 and 350 degrees. Using the optimized geometries for the different adsorption modes, electronic structure calculations were also performed to obtain the projected density-of-states (PDOS) profiles. The contribution to the total DOS for the lowest-unoccupied molecular orbital (LUMO) of each branch in **2**@TiO_2 was separated and the interaction between the dye and the semiconductor was analyzed following the Newns–Anderson model.[49,50] The normalized contribution, p_i, to the PDOS relative to the dye's LUMO is defined as the portion of the ψ_i molecular orbital located on the sensitizer, evaluable by the relation:

$$p_i = \frac{\sum_{j}^{A\in dye} \left(c_{ij}^{A}\right)^2}{\sum_{j}^{n} \left(c_{ij}^{A}\right)^2} \quad (1)$$

where c_{ij}^{A} values are the expansion coefficients when ψ_i is expressed as a linear combination of n atomic orbitals centered on atom A.

To ensure that the PDOS belongs to the sensitizer's LUMO we selected a number of abduct orbitals so that the $\sum p_i \approx 1$. Since there are two nearly degenerate LUMOs due to the presence of two branches in the **2**@TiO_2 system, only the contribution to the DOS of the branch "better" linked to the semiconductor surface was taken into account for the fitting. The center of this distribution corresponds to the energy of the LUMO of the dye adsorbed on TiO_2, $E_{LUMO}(ads)$, and it can be calculated as

$$E_{LUMO}(ads) = \sum_i p_i \varepsilon_i \quad (2)$$

where ε_i values are the orbital energies of the combined system for the selected energy range. The LUMO broadening has been then obtained as a mean deviation of a distribution centered at the $E_{LUMO}(ads)$:

$$\hbar\Gamma = \sum_i p_i |\varepsilon_i - E_{LUMO}(ads)| \quad (3)$$

The energetic distribution of the LUMO for the dye adsorbed on the TiO_2 has been fitted using a Lorentzian function:

$$\rho_{LUMO}(E) = \frac{1}{\pi} \frac{\left(\frac{\hbar\Gamma}{2}\right)}{(E - E_{LUMO}(ads))^2 + \left(\frac{\hbar\Gamma}{2}\right)^2} \quad (4)$$

In this model, the LUMO broadening gives a direct estimation of the electron-transfer time by the relation:

$$\tau(fs) = \frac{658}{\Gamma(meV)} \quad (5)$$

3. Results and discussion

3.1. Molecular calculations: simple models

To evaluate the possibility of reducing the molecular size of the dye to study the adsorption mode on the semiconductor, frequency calculations were first performed at the B3LYP/6-31G* level for the entire dye under study (**A**) and for the two size-reduced molecular models **1** and **2**, which incorporate one and two anchoring groups, respectively (see Fig. 1). The 10-(1,3-dithiol-2-ylidene)anthracene moiety, the donor part of dye **A**, is fully suppressed in **1** and **2**. These preliminary calculations allow us to assess how the vibrational modes that characterize the anchoring region evolve in passing from the reduced systems to the entire molecule. The vibrational frequencies calculated for **1** and **2** are compared to those obtained for **A** in Fig. 3.

An overall correspondence is found for the vibrational modes calculated in the 1000–1800 cm^{-1} range, which increase in intensity passing from **1** to **2** and to **A** (Fig. 3). The peak above 1700 cm^{-1} corresponds to the C═O stretching mode and the intense transition around 1570 cm^{-1} is associated with a C═C stretching. For **A**, a relative intense transition is computed at 1480–1500 cm^{-1} which corresponds to C═C stretching modes in the donor moiety. Less intense bands can be found for **1**, **2** and **A** in the 1400–1500 cm^{-1} region which are assigned to aromatic C–C–H bendings. The peak computed at 1340 cm^{-1} results from the intense stretching of the C–OH bond plus some weaker aromatic C–C–H bending modes. A low intense transition appears for **A** at around 1260 cm^{-1} that corresponds to C–C–H bendings of the anthracene part. Finally, the high-intense peak at 1140 cm^{-1} is due to the C–O–H bending. Therefore, the characteristic modes of the carboxylic group in the IR spectrum are repeated along the series of compounds **1**, **2** and **A** in their neutral form. The same behavior is expected for different anchoring modes, so that it is possible to extrapolate the vibrational properties of **A** in a particular adsorption mode from those of **1**, except for some low-intense transitions that are associated with the donor moiety.

To investigate the adsorption coordination of compound **1** onto the TiO_2 surface, six possible structural environments

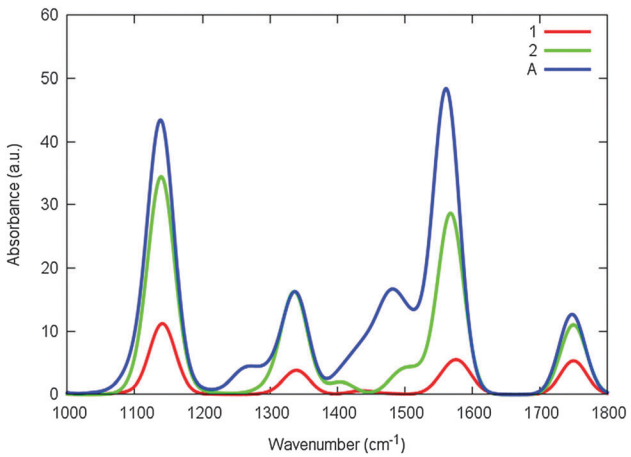

Fig. 3 IR spectra computed for the neutral species of system **A** and subsystems **1** and **2**.

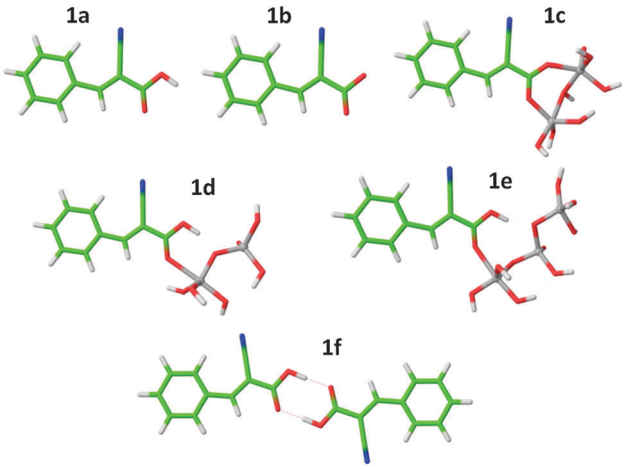

Fig. 4 Optimized geometries of compound **1** in different structural environments. Atom colors: C in green, O in red, H in white, N in blue and Ti in grey.

were modeled taking into account the nature of the carboxylic group: neutral (**1a**), anion (**1b**), linked to a $Ti_2O_7H_6$ cluster in BB- (**1c**) and M2-like (**1d**) adsorption modes, linked to a $Ti_3O_{10}H_8$ cluster in an M1-like coordination (**1e**) and as a dimer (**1f**). The comparison of the frequencies calculated for these structures allows the determination of general trends for the IR bands associated with the $COOH/COO^-$ group in passing from the isolated system (**1a** and **1b**) through a monodentate linkage (**1d** and **1e**) to a bidentate-like (**1c**) mode. The optimized structures computed in the gas phase for structures **1a–1f** are shown in Fig. 4.

The main differences concerning the vibration modes of the anchoring group between systems **1a–1f** are found in the 1000–1800 and 3000–3600 cm^{-1} regions (see Fig. S1 in the ESI† for the 1000–1800 cm^{-1} region). The O–H stretching appears beyond 3500 cm^{-1}, except for **1b**, and it drops around 500 cm^{-1} in **1d**, **1e** and **1f** due to the formation of hydrogen bonds. As far as CO characteristic modes are concerned, the symmetric and asymmetric stretching of the $COOH/COO^-$ group are fairly intense in the IR spectrum and their position, as stated in the introduction, represents an indication of the anchoring topology. The symmetric stretching is predicted in the 1250–1450 cm^{-1} region and there is no clear trend passing from monodentate- to bidentate-like anchorages (Table 1). The asymmetric stretching

Table 1 Infrared frequencies (in cm^{-1}) calculated for the main vibrational modes of structures **1a–1f** at the B3LYP/6-31G* level of theory (gas phase), and obtained from the experimental IR spectra of dye **A** as a powder and adsorbed onto TiO_2

System	CO asymm	CO symm	C═C	C–C–H	$\Delta\nu_{as}$ [a]
1a	1750	1340	1570	1340	410
1b	1710	1260	1590	1330	450
1c	1550	1390	1590	1350	150
1d	1650	1440	1570	1360	210
1e	1660	1400	1570	1360	260
1f	1700	1420	1570	1360	280
Exp. **A** powder [b]	1710	1420	1590	1350	290
Exp. **A**@TiO_2 [b]	1620	1390	1590	1350	230

[a] $\Delta\nu_{as} = \nu$(CO asymm) – ν(CO symm). [b] IR spectra from ref. 25.

is computed at larger wavenumbers, in the 1550–1750 cm^{-1} region. Calculations indicate that the more monodentate character of the linkage, the higher the energy of the asymmetric mode. This leads to a $\Delta\nu_{as}$ > 200 cm^{-1} for monodentate coordinations (**1d** and **1e**) whereas a value below 200 cm^{-1} is obtained for the bidentate anchorage (**1c**). Intense vibrational transitions associated with the aromatic backbone of the dye grow in the same region as the CO stretchings and constitute a difficulty in the correct experimental assignation of the symmetric and asymmetric CO modes. C=C stretchings are computed around at 1550–1600 cm^{-1} and can compete in intensity and position with the asymmetric CO stretching, especially for the bidentate coordinations (see Table 1). Moreover, an aromatic C–C–H bending mode is predicted at around 1350 cm^{-1} and its position is well preserved over all the models. This vibration may overlap the symmetric CO stretching in both monodentate- and bidentate-like anchoring environments, but it is computed at lower energies in all cases except for the non-representative **1b**. Theoretical frequency calculations therefore allow the unequivocal assignation of the characteristic CO modes in the experimental IR spectrum reported by Bouit *et al.*,[25] leading to the values shown in Table 1 for **A** as a powder and adsorbed on TiO_2. The theoretical frequencies calculated for **1f** nicely fit the experimental data for the dye as a powder suggesting that the dye forms dimers in the powder as occurs in other cyanoacrylic acid-based compounds.[51] The experimental value of $\Delta\nu_{as}$ = 290 cm^{-1} inferred for the dye as a powder compared to the 280 cm^{-1} value predicted for **1f** supports this assumption. In turn, vibrational assignation of the **A**@TiO_2 modes opens the door to more than one model. The experimental value of $\Delta\nu_{as}$ = 230 cm^{-1} resulting from the theoretical assignment suggests that monodentate coordinations ($\Delta\nu_{as}$ of 210 and 260 cm^{-1} for **1d** and **1e**, respectively) are more likely to provide the real coordination in the **A**@TiO_2 system than a bidentate adsorption mode (**1c**, $\Delta\nu_{as}$ = 150 cm^{-1}). Moreover, a better match of the CO symmetric mode calculated for **1e** (1400 cm^{-1}) with the corresponding **A**@TiO_2 mode (1390 cm^{-1}) points to the M1 adsorption as the more likely coordination mode.

A parallel series of calculations was also performed using the PBE0 functional and the scaled results (scaling factor of 0.986) were almost identical to the B3LYP calculations (Fig. S2, ESI†). Therefore, no qualitative or quantitative difference upon changing the functional for the analysis of the vibrational modes in our systems is expected. PCM calculations in acetonitrile solution were also performed showing the same qualitative trends with a general increase in intensity for the CO and C=C stretching transitions (Fig. S3 and S4, ESI†).

3.2. Periodic calculations

(a) Geometry analysis. Having established the relationship between the characteristic normal modes of the $COOH/COO^-$ group and its environment, we can now move to model the di-branched system **2** (Fig. 1) anchored to the anatase (101) surface. Four single-anchored adsorption configurations, *i.e.* three monodentate (M1, M2 and MN) and one bidentate (BB) structures, and two di-anchored conformations, *i.e.* one monodentate (M1–M1) and one bidentate (BB–BB) structures, were considered (Fig. 5). All the conformations were fully optimized using the Car–Parrinello algorithm and the most relevant geometrical parameters are given in Table 2. The M1–M1 conformation was optimized before and after running a long *ab initio* molecular dynamics simulation (termed M1–M1(before) and M1–M1(after) in Fig. 5).

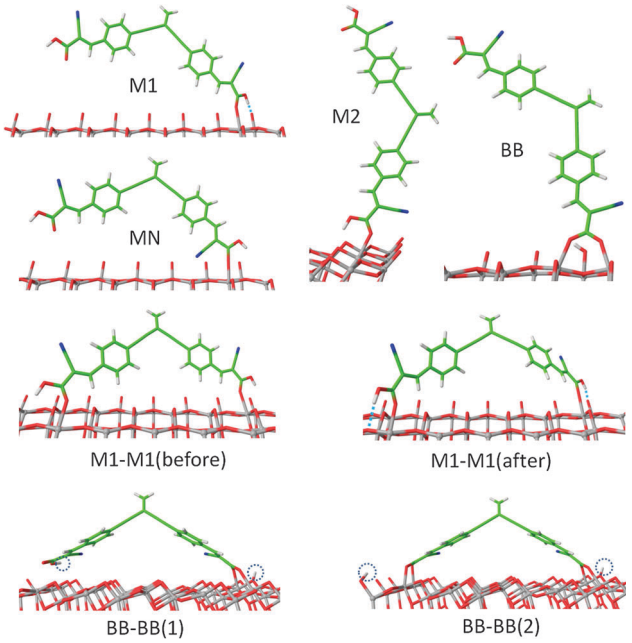

Fig. 5 Adsorption conformations modeled for system **2**. M1–M1(before) and M1–M1(after) correspond to minimum-energy conformations optimized before and after the *ab initio* molecular dynamics simulation.

Among the single-anchored systems, it is worth differentiating between the monodentate and the bidentate systems: while in the M1, M2 and MN adsorptions a different length is calculated for the $C–O_1$ and $C–O_2$ bonds, in the BB adsorption the situation is completely symmetric (Table 2). M1 and M2 only differ in the

Table 2 Selected bond distances (in Å) for the different conformations of **2**@TiO_2

Structure	$Ti_1–O_1$ ($Ti_2–O_2$)	$C–O_1$	$C–O_2$	$O_2–H$	$H\cdots O_{3/4}$	$N–Ti_2$	N–H
M1	2.248	1.249	1.321	1.030	1.546	—	—
M2	2.239	1.250	1.333	1.019	1.687	—	—
MN	2.129	1.231	1.347	0.983	—	2.616	—
BB	2.157 (2.254)	1.285	1.285	—	0.980	—	—
M1–M1(before)[a]	2.364	1.237	1.346	0.988	2.335	—	—
	2.228	1.242	1.343	0.986	3.202	—	—
M1–M1(after)[a]	2.256	1.245	1.331	1.012	1.731	—	—
	2.171	1.251	1.334	1.003	1.889	—	—
BB–BB(1)[a]	2.152 (2.317)	1.289	1.287	—	0.976	—	—
	2.713 (2.862)	1.225	1.366	0.988	2.160	—	2.448
BB–BB(2)[a]	2.127 (2.116)	1.282	1.298	—	0.974	—	—
	2.626 (2.074)	1.254	1.319	—	0.978	—	—

[a] Values corresponding to each anchoring branch of **2** are given in different rows.

oxygen type (O_4 and O_3, respectively) to which the carboxylic acid is H-bonded. The shorter value calculated for the bond length between the carboxylic hydrogen and the O_3/O_4 atoms ($H\cdots O_{3/4}$) suggests a stronger hydrogen bond interaction in the case of M1. In both cases, the hydrogen is retained by the carboxylate group and it is not transferred to the TiO_2 surface. A recent work has demonstrated that the inclusion of solvent effects slightly modifies the H-transfer scenario: more polar solvents favor the H-transfer to the semiconductor.[29] The MN structure was included in the analysis because here it competes in energy with M1 and M2 (*vide infra*), although it is usually computed higher in energy.[16,18,19,31,33,45,52–63] As shown in Table 2, this conformation presents a relatively small N–Ti distance of 2.62 Å, which contributes to the relative stabilization of the adsorption mode. A comparison of the relative energies for the different adsorption modes will be discussed below.

The doubly anchored conformations deserve particular attention since, in line with previous findings on di-branched dyes,[22] the experimental FTIR spectra suggest that our di-branched dye is attached to the TiO_2 surface by means of both anchoring groups.[25] In the optimized M1–M1(after), the $C–O_1$ bond lengthens and the $C–O_2$ bond shortens compared to M1–M1(before), thus the carboxylate group attains a more symmetric disposition. This is due to the formation of a hydrogen bond with the $O_{3/4}$ as a consequence of the rearrangement of the molecule after the dynamics. The $H\cdots O_{3/4}$ distance shortens in passing from M1–M1(before) to M1–M1(after) clearly pointing to the formation of a hydrogen bond. Moreover, the distortion from planarity to form the H-bond suggests that the energy stabilization due to the formation of the H-bond is much higher than the energy destabilization due to the partial breaking of planarity. The longer $H\cdots O_{3/4}$ distance predicted for M1–M1(after) compared to M1 and M2 is a signal of the geometrical constraints that M1–M1 suffers to be anchored adequately by its two cyanoacrylic acid groups forming two stabilizing H-bonds. Fig. 6 displays the evolution of the $O_2–H$ and $H\cdots O_{3/4}$ distances over time during the CP molecular dynamics. As shown, the temperature is high enough to break and form again the bonds involving the carboxylic hydrogen, thus giving flexibility to the system to explore a huge zone of the potential energy surface. At around 1.25–1.50 ps, the $H\cdots O_{3/4}$ distance presents large values indicating a breaking of the H-bond (Fig. 6), whereas at 0.75 and 2.30 ps, the shorter distance predicted for $H\cdots O_{3/4}$ than for $O_2–H$ suggests a proton transfer from the carboxylic acid to the semiconductor oxygen. The exploration of the possible conformations of the di-branched dye therefore shows that, on average, the M1–M1 adsorption structure is the most visited disposition.

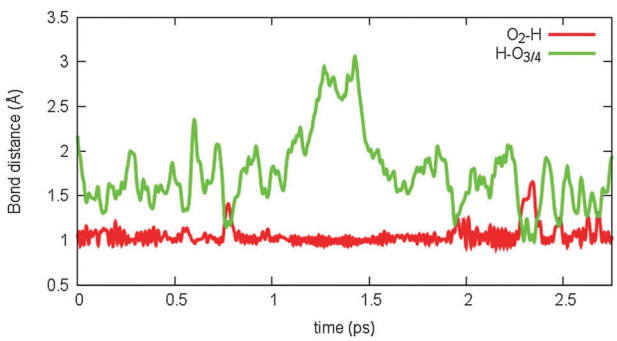

Fig. 6 Time evolution of the characteristic $O_2–H$ and $H\cdots O_{3/4}$ bond distances during the Car–Parrinello molecular dynamics simulation.

An additional geometrical distortion from planarity has to be made in order to obtain the BB–BB adsorption conformation, in which the dye is lying along the semiconductor surface. To generate this conformation, the two anchoring branches of the molecule need to adopt a perpendicular orientation with respect to the central $C{=}CH_2$ unit and lose the π-connection between them (see Fig. 5). Depending on the position of the carboxylic hydrogen of one branch in the semiconductor surface, we distinguish two clearly different situations: BB–BB(1), where the H is kept bonded to the anchoring group of the dye, and BB–BB(2), where the H is displaced to be linked to a further $O_{3/4}$ of the semiconductor. Whereas distance parameters are mostly equal in the purely BB branch for both situations, a significant difference is observed in the other branch where a competition between an M1 and a BB mode appears due to the relative position of the hydrogen atom (Table 2). In BB–BB(1), the H remains linked to the carboxylic acid and forms a kind of double H-bond with the N atom of the cyano group (N–H distance: 2.448 Å) and the $O_{3/4}$ atom ($H\cdots O_{3/4}$ distance: 2.16 Å). This mode possesses an asymmetric situation for the C–O bonds (1.225 and 1.366 Å) resembling a monodentate mode. For BB–BB(2), both anchoring groups provide a BB chelation but while one group is well bonded to the surface (2.127 and 2.116 Å for Ti–O distances), the other group has only a strong interaction through one oxygen (2.626 and 2.074 Å for Ti–O distances) due to the rigidity of the system.

(b) Relative stabilities. To shed light on the energetics of the different possible structures for the combined dye@TiO_2 system, we calculated the relative energy of the modeled conformations with different adsorption modes (Table 3) using the Car–Parrinello optimized geometries. Two different periodic slabs were used to model the conformations here compared, and the energies between conformations held on different slabs have been related through the energy difference between the two isolated TiO_2 slabs. The reliability of this approach was confirmed by calculating the same conformation (structure M1) on the two $(TiO_2)_n$ slabs (n = 64 and 72). The energy difference

Table 3 Relative stabilities of the modeled adsorption conformations for **2**@TiO_2

Structure	Relative energy (kcal mol^{-1})
M1	4.98
M2	3.70
MN	9.70
BB	14.16
M1–M1(before)	0.00
M1–M1(after)	−9.39
BB–BB(1)	30.27
BB–BB(2)	38.55

obtained between the two calculations using the energy difference between the isolated slabs was as small as 0.30 kcal mol^{-1}.

The energy calculated for the M1–M1(before) structure is taken as a reference. Among the four single-anchored conformations, M2 is calculated to be the most stable adsorption mode, with the M1 structure being quite close in energy (1.28 kcal mol^{-1}). However, taking into account the spatial arrangement of the COOH groups (Fig. 5), a di-anchored M2–M2 conformation is not feasible due to the geometric rigidity of the dye and it was therefore not modeled. The MN adsorption mode also gives a relatively small energy and is found to be 6.00 kcal mol^{-1} less stable than M2. The bridging bidentate (BB) mode is computed to be more than 10 kcal mol^{-1} higher in energy than M2, in good agreement with previous theoretical studies employing Car–Parrinello calculations using periodic boundary conditions.[17,64] Moving to the di-anchoring conformations, M1–M1(before) stands much more stable than BB–BB (30 kcal mol^{-1}). Furthermore, after the molecular dynamics simulation and the corresponding reoptimization procedure, M1–M1(after) gains an extra stabilization of more than 9 kcal mol^{-1} compared to M1–M1(before). This additional stability is a consequence of the formation of two H-bonds upon deformation of the dye structure from planarity. BB–BB(1) and BB–BB(2) therefore lie much higher in energy than M1–M1. In fact, the di-anchored BB structures are less stable than the single-anchored BB conformation by more than 15 kcal mol^{-1}. This huge destabilization is due to the inefficient bond interactions caused by the rigid structure of the dye, the fixed topology of the TiO_2 surface and the additional π-conjugation breaking experienced by the dye to adopt the di-anchored BB structures. In passing from M1 to M1–M1(after) a stabilization of around 14 kcal mol^{-1} is obtained for the di-anchored conformation, which mostly corresponds to the energy gain associated with the anchorage of a carboxylic acid group to the anatase (101) surface ($\sim$18.5 kcal mol^{-1}).[64] Based on the present calculations, which might however overstabilize the monodentate anchoring, dye **A** is therefore found to adsorb on the TiO_2 surface in a di-anchored monodentate M1–M1 manner in good agreement with experimental suggestions based on IR spectra.[25]

(c) Electronic structure. To gain insight into the influence of the anchoring process on the electronic features of the final DSC device, we studied the density of states (DOS) for both the bare periodic slab and the dye@TiO_2 models using the PBE functional. Calculations were performed on the M1, M1–M1, BB and BB–BB structures optimized for **2**, which should provide a reliable description of the adsorbed systems because it contains both anchoring groups at the relative distance they have in the entire dye. Special attention must be paid to the relative energy position of the conduction band and the LUMO, whereas no concluding remarks should be taken from the valence band (VB) and the HOMO positions due to the lack of the donor moiety in model **2**. The presence of the donor moiety might also influence the CB position because it modulates the charge transfer (CT) in the ground state to the semiconductor as recently proved.[65] However, since theoretical calculations demonstrated negligible donor–acceptor CT in the ground state

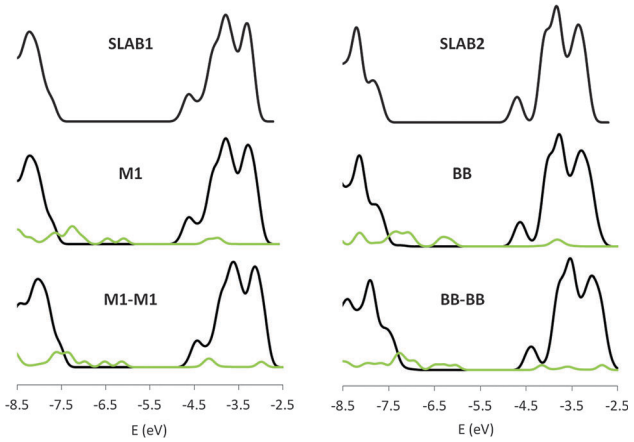

Fig. 7 Projected density of states (PDOS) calculated for the M1, M1–M1, BB and BB–BB adsorption models of **2**@TiO_2 and for their respective bare periodic slabs. Black and green lines represent the contribution of the semiconductor surface and the adsorbed molecule, respectively, to the density of states.

for the isolated compounds **A** and **B**,[25] and we are interested in relative changes for the different adsorption modes in the same system, no special concern has been shown to include the donor moiety. The absolute energy of the bands in the DOS diagram was calculated by referring the Kohn–Sham eigenvalues to the vacuum level, as determined from the value of the electrostatic potential in the vacuum region of the supercell. Electrostatic potentials along the direction normal to the surface for the dye-sensitized TiO_2 slab are included in the ESI† (Fig. S5 and S6).

Fig. 7 shows the projected density of states (PDOS) decomposition of the total DOS to highlight the role of the adsorption mode in the energy level distribution, and Table 4 collects the most relevant energy data. A band gap of 2.6 eV is computed for both bare model slabs, which is slightly underestimated compared to the experimental value of $\sim$3.0 eV reported elsewhere.[66,67] This result evidences the well-established shortcoming of standard DFT calculations leading to the underestimation of the band gap in semiconductors.[68]

Single-anchoring modes such as M1 and BB maintain unchanged the position of the CB in the bare slab (−4.9 eV),

Table 4 Energy (eV) for the main bands close to the Fermi level obtained from the periodic calculations

	SLAB1	M1	M1–M1	SLAB2	BB	BB–BB
LUMO(1)[a]	—	−4.1	−4.2	—	−3.8	−3.6
LUMO(2)[a]	—	−4.0	−4.1	—	−3.8	−4.1
CB	−4.9	−4.9	−4.7	−4.9	−4.9	−4.6
VB	−7.5	−7.5	−7.4	−7.5	−7.5	−7.2
Band gap	2.6	2.6	2.7	2.6	2.6	2.6
LUMO–CB[b]	—	0.8	0.5	—	1.1	1.0

[a] LUMO(1) and LUMO(2) refer to the PDOS contribution to the total DOS for the better-anchored branch and the worse- or non-anchored branch of **2** in the **2**@TiO_2 system, respectively. [b] The LUMO(1) is used in the difference since it is the one which most participates in the electron injection process into the semiconductor.

whereas di-anchored adsorptions M1–M1 and BB–BB slightly shift the CB to higher energies by 0.2 and 0.3 eV, respectively (Table 4). As previously described, the sensitizer's dipole component normal to the surface induces a shift in the TiO_2 CB energy.[31,69] Actually, the situation is more entangled and some of us have recently shown that the CB shift is the result of a combined effect of (i) the amount of electron density transferred in the ground state from the dye to the semiconductor and (ii) the electric field generated by the dye on the TiO_2 surface.[65] Therefore, di-anchored models, where the two branches are linked to the semiconductor, show larger CT and electric field effects with respect to the single-anchored systems thus shifting the CB at a larger extent. An even sustained shift for the CB is expected when considering the entire dye due to an enhancement of the above-mentioned electronic features provoked by the donor group.

As far as the PDOS corresponding to the molecule adsorbed is concerned, special care must be taken since the two identical branches of the dye present different environments, thus leading to non-degenerate LUMO energy levels (see Table 4 and Fig. S7, ESI†). A splitting in the degeneracy in LUMO(1) and LUMO(2) is computed for M1 where the carboxylic acid of the anchoring group binds to the semiconductor surface, whereas near-degeneracy is predicted for M1–M1 due to the almost equivalent anchoring topology. Accidentally, these bands are almost degenerate in energy for BB (see Table 4) but the different width computed for each one unequivocally determines the contribution (LUMO(1)) of the anchored branch (Fig. S7, ESI†). Finally, the energy difference between the two LUMOs is computed to be 0.6 eV (see Table 4), due to the completely different arrangement of the $COOH/COO^-$ groups on the TiO_2 surface (*vide supra* in the Geometry Analysis). In the same geometrical environments, a slight decrease in energy is predicted for the LUMO band corresponding to the better interacting branch (from −4.0 and −4.1 to −4.2 in M1 and M1–M1, respectively). This trend does not apply to the dissociative bridged bidentate adsorptions due to the different $COOH/COO^-$ nature in the two branches.

Since the system under study possesses two near-degenerate unoccupied molecular orbitals (LUMO(1) and LUMO(2) in Table 4) in the 2@TiO_2 association, the PDOS corresponding to the better anchored branch LUMO(1) was extracted due to its relevant role on the electron injection into the semiconductor. The PDOS for the LUMO(1) was fitted to a Lorentzian peak function in order to quantify the interaction of the dye with the semiconductor. As shown in Fig. 8, the BB adsorption provides a wider band width (0.184 eV) compared to M1 (0.147 eV). The broadening of the LUMO of the dye is directly related to its interaction with the CB states of the TiO_2. Thus, the BB adsorption would be expected to provide a faster electron injection into the semiconductor.[57] Likewise, the BB–BB adsorption fit computes a broader LUMO band than M1–M1 thus favoring the electron injection. According to expression (5), we calculate electron-transfer times of 4.5, 3.6, 4.7 and 4.2 fs for M1, BB, M1–M1 and BB–BB, respectively. Obviously, the width of the LUMO band in the singly anchored conformations

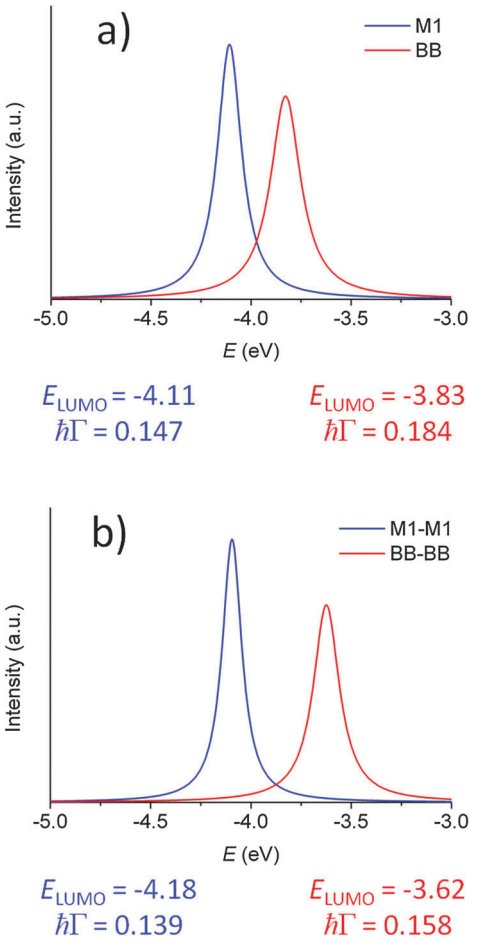

Fig. 8 Lorentzian fitting of the PDOS corresponding to the LUMO of the better anchored branch in the system **2**@TiO_2 for the singly (a) and doubly (b) anchored adsorption modes. The corresponding fitting parameters E_{LUMO} (center of the peak) and $\hbar\Gamma$ (full width at half-peak height) of the Lorentzian function according to the expression (4) are displayed.

is wider than in the doubly anchored ones since the branch we are analyzing is better accommodated on the TiO_2 surface in the former. However, notice that this broadening effect is doubled in M1–M1 and BB–BB adsorption modes thus resulting in an enhanced electron injection into the semiconductor.

A rule of thumb for obtaining efficient electron injections in DSCs is to have a dye that provides an energy difference between LUMO and CB of around 0.5 eV. In this way, M1 and especially M1–M1 offer good LUMO–CB gaps (0.7 and 0.5 eV, respectively) for efficient electron injection. Therefore, the doubly anchored M1–M1 structure has two positive effects on the electronic properties: (i) it produces an increase in the CB energy, which should be beneficial for the DSCs performance in terms of an increase of the open circuit voltage, and (ii) it enhances the dye-semiconductor interaction leading to a broadening of the LUMOs and an adequate LUMO–CB gap, which favors electron injection into the semiconductor. It is thus evidenced that multi-anchored systems better fulfill the electronic requirements for DSCs and offer the possibility of modulating the LUMO–CB energy difference in a systematic way depending on the number of anchoring groups.

4. Conclusions

A first-principles investigation has been performed to determine the anchoring mode of an exTTF-based, di-branched, donor–acceptor dye to the anatase (101) surface. Considering two reduced but still reliable dye subsystems, a number of different anchoring environments were designed to determine not only the position of the symmetric and asymmetric CO stretching modes but also other vibrations appearing at similar energies, which may hinder the assignment of the diagnostic COOH/COO^- modes. The theoretical characterization of the typical vibrational modes in a dye@TiO_2-like system enabled the firm assignation of the symmetric and asymmetric CO modes in the available experimental FTIR spectrum. The comparison of the $\Delta\nu_{as}$ values inferred from the experiment and those theoretically obtained for the **1a–1f** models suggests that, whereas the dye forms dimers in the powder, it adsorbs on the semiconductor surface most likely in an M1 monodentate coordination.

The reduced system **2**, which contains the two anchoring groups present in the entire dye **A**, was used to perform optimizations of the most relevant COOH/COO^- coordinations over a periodic slab of anatase (101). Singly anchored monodentate adsorptions (M1, M2 and MN) are computed lower in energy than the bridging bidentate (BB) adsorption, in line with previous Car–Parrinello PBC results.[17] Doubly anchored monodentate M1–M1 structures provide a gain in stability with respect to the singly anchored analogue. Exploring the potential energy surface by means of a Car–Parrinello molecular dynamics along 3 ps, we arrive at an M1–M1 structure in which the carboxylic anchoring groups are better positioned on the TiO_2 surface and form two stabilizing H-bonds. This structure, being about 14 kcal mol^{-1} lower in energy than the monodentate M1 structure, corresponds to the most stable adsorption conformation. BB–BB adsorptions have been shown to be much higher in energy than M1–M1 not only because of the total breaking of the π-conjugation between the two acceptor branches but especially for the inadequate match of the carboxylic groups with respect to the anatase (101) topology. Therefore, the doubly anchored, monodentate M1–M1 structure is predicted as the energetically favored adsorption in good agreement with experimental evidences.

The projected density of states calculated for M1, BB, M1–M1 and BB–BB adsorption modes predict that the doubly anchored systems shift the conduction band of TiO_2 to slightly higher energies compared to the singly anchored analogues. This shift allows for an increase in the open-circuit voltage permitting higher conversion efficiencies for DSC purposes. Moreover, an extensive analysis of the PDOS for the different branches in the **2**@TiO_2 system allowed the understanding of the inner role for the two nearly degenerate LUMO bands corresponding to the two identical branches of the dye in the total DOS. Although the singly anchored M1 adsorption provides a slightly broader LUMO band due to the better anchoring disposition onto TiO_2, the broadening in M1–M1 is doubled since the two branches are well interacting with the semiconductor surface. Overall, the energetically favored M1–M1 structure provides appropriate LUMO–CB energy differences with two broad and intense LUMO bands, which favor the electron injection into the semiconductor and explains the good performance experimentally achieved in the device.

Acknowledgements

MP, EM and FDA thank CNR Projects EFOR and RADIUS, and FP7-ENERGY-2010 project 261920 "ESCORT" for financial support. JC and EO thank the MINECO of Spain and European FEDER funds (project CTQ2012-31914) and the Generalitat Valenciana (Prometeo/2012/053). JC acknowledges the Ministry of Education, Culture and Sport (MECS) of Spain for a FPU grant.

References

1 A. Hagfeldt, G. Boschloo, L. Sun, L. Kloo and H. Pettersson, *Chem. Rev.*, 2010, **110**, 6595–6663.
2 M. K. Nazeeruddin, F. De Angelis, S. Fantacci, A. Selloni, G. Viscardi, P. Liska, S. Ito, B. Takeru and M. Grätzel, *J. Am. Chem. Soc.*, 2005, **127**, 16835–16847.
3 B. O'Regan and M. Gratzel, *Nature*, 1991, **353**, 737–740.
4 M. K. Nazeeruddin, A. Kay, I. Rodicio, R. Humphry-Baker, E. Mueller, P. Liska, N. Vlachopoulos and M. Graetzel, *J. Am. Chem. Soc.*, 1993, **115**, 6382–6390.
5 A. Mishra, M. K. R. Fischer and P. Bäuerle, *Angew. Chem., Int. Ed.*, 2009, **48**, 2474–2499.
6 M. Pastore, E. Mosconi, S. Fantacci and F. De Angelis, *Curr. Org. Chem.*, 2012, **9**, 215–232.
7 D. P. Hagberg, J.-H. Yum, H. Lee, F. De Angelis, T. Marinado, K. M. Karlsson, R. Humphry-Baker, L. Sun, A. Hagfeldt, M. Grätzel and M. K. Nazeeruddin, *J. Am. Chem. Soc.*, 2008, **130**, 6259–6266.
8 H. Choi, C. Baik, S. O. Kang, J. Ko, M.-S. Kang, M. K. Nazeeruddin and M. Grätzel, *Angew. Chem., Int. Ed.*, 2008, **47**, 327–330.
9 G. Zhang, Y. Bai, R. Li, D. Shi, S. Wenger, S. M. Zakeeruddin, M. Gratzel and P. Wang, *Energy Environ. Sci.*, 2009, **2**, 92–95.
10 J.-H. Yum, E. Baranoff, F. Kessler, T. Moehl, S. Ahmad, T. Bessho, A. Marchioro, E. Ghadiri, J.-E. Moser, C. Yi, M. K. Nazeeruddin and M. Grätzel, *Nat. Commun.*, 2012, **3**, 631.
11 E. Mosconi, J.-H. Yum, F. Kessler, C. J. Gómez García, C. Zuccaccia, A. Cinti, M. K. Nazeeruddin, M. Grätzel and F. De Angelis, *J. Am. Chem. Soc.*, 2012, **134**, 19438–19453.
12 A. Yella, H.-W. Lee, H. N. Tsao, C. Yi, A. K. Chandiran, M. K. Nazeeruddin, E. W.-G. Diau, C.-Y. Yeh, S. M. Zakeeruddin and M. Grätzel, *Science*, 2011, **334**, 629–634.
13 T. Daeneke, T.-H. Kwon, A. B. Holmes, N. W. Duffy, U. Bach and L. Spiccia, *Nat. Chem.*, 2011, **3**, 211–215.
14 S. M. Feldt, E. A. Gibson, E. Gabrielsson, L. Sun, G. Boschloo and A. Hagfeldt, *J. Am. Chem. Soc.*, 2010, **132**, 16714–16724.
15 M. Pastore and F. De Angelis, *Top. Curr. Chem.*, 2013, DOI: 10.1007/128_2013_468.

16 A. Vittadini, A. Selloni, F. P. Rotzinger and M. Grätzel, *J. Phys. Chem. B*, 2000, **104**, 1300–1306.
17 C. Anselmi, E. Mosconi, M. Pastore, E. Ronca and F. De Angelis, *Phys. Chem. Chem. Phys.*, 2012, **14**, 15963–15974.
18 F. De Angelis, S. Fantacci, A. Selloni, M. K. Nazeeruddin and M. Grätzel, *J. Phys. Chem. C*, 2010, **114**, 6054–6061.
19 F. De Angelis, S. Fantacci, A. Selloni, M. Grätzel and M. K. Nazeeruddin, *Nano Lett.*, 2007, **7**, 3189–3195.
20 C. Y. Lee, C. She, N. C. Jeong and J. T. Hupp, *Chem. Commun.*, 2010, **46**, 6090–6092.
21 R. Sirohi, D. H. Kim, S.-C. Yu and S. H. Lee, *Dyes Pigm.*, 2012, **92**, 1132–1137.
22 A. Abbotto, N. Manfredi, C. Marinzi, F. De Angelis, E. Mosconi, J.-H. Yum, Z. Xianxi, M. K. Nazeeruddin and M. Gratzel, *Energy Environ. Sci.*, 2009, **2**, 1094–1101.
23 S. Wenger, P.-A. Bouit, Q. Chen, J. Teuscher, D. D. Censo, R. Humphry-Baker, J.-E. Moser, J. L. Delgado, N. Martín, S. M. Zakeeruddin and M. Grätzel, *J. Am. Chem. Soc.*, 2010, **132**, 5164–5169.
24 A. S. Batsanov, M. R. Bryce, M. A. Coffin, A. Green, R. E. Hester, J. A. K. Howard, I. K. Lednev, N. Martín, A. J. Moore, J. N. Moore, E. Ortí, L. Sánchez, M. Savirón, P. M. Viruela, R. Viruela and T.-Q. Ye, *Chem.–Eur. J.*, 1998, **4**, 2580–2592.
25 P.-A. Bouit, M. Marszalek, R. Humphry-Baker, R. Viruela, E. Ortí, S. M. Zakeeruddin, M. Grätzel, J. L. Delgado and N. Martín, *Chem.–Eur. J.*, 2012, **18**, 11621–11629.
26 M. Xu, S. Wenger, H. Bala, D. Shi, R. Li, Y. Zhou, S. M. Zakeeruddin, M. Grätzel and P. Wang, *J. Phys. Chem. C*, 2009, **113**, 2966–2973.
27 G. Zhang, H. Bala, Y. Cheng, D. Shi, X. Lv, Q. Yu and P. Wang, *Chem. Commun.*, 2009, 2198–2200.
28 M. Planells, L. Pelleja, J. N. Clifford, M. Pastore, F. De Angelis, N. Lopez, S. R. Marder and E. Palomares, *Energy Environ. Sci.*, 2011, **4**, 1820–1829.
29 M. Nara, H. Torii and M. Tasumi, *J. Phys. Chem. A*, 1996, **100**, 19812–19817.
30 M. Pastore and F. D. Angelis, *ACS Nano*, 2009, **4**, 556–562.
31 P. Chen, J. H. Yum, F. D. Angelis, E. Mosconi, S. Fantacci, S.-J. Moon, R. H. Baker, J. Ko, M. K. Nazeeruddin and M. Grätzel, *Nano Lett.*, 2009, **9**, 2487–2492.
32 H. Tian, X. Yang, R. Chen, R. Zhang, A. Hagfeldt and L. Sun, *J. Phys. Chem. C*, 2008, **112**, 11023–11033.
33 M. Pastore and F. D. Angelis, *J. Phys. Chem. Lett.*, 2011, **2**, 1261–1267.
34 F. Nunzi and F. De Angelis, *J. Phys. Chem. C*, 2010, **115**, 2179–2186.
35 G. B. Deacon and R. J. Phillips, *Coord. Chem. Rev.*, 1980, **33**, 227–250.
36 A. D. Becke, *J. Chem. Phys.*, 1993, **98**, 5648–5652.
37 P. J. Stephens, F. J. Devlin, C. F. Chabalowski and M. J. Frisch, *J. Phys. Chem. A*, 1994, **98**, 11623–11627.
38 J. Tomasi and M. Persico, *Chem. Rev.*, 1994, **94**, 2027–2094.
39 C. S. Cramer and D. G. Thrular, *Solvent Effects and Chemical Reactivity*, Kluwer, Dordrecht, 1996.
40 C. A. Jimenez-Hoyos, B. G. Janesko and G. E. Scuseria, *Phys. Chem. Chem. Phys.*, 2008, **10**, 6621–6629.
41 J. P. Merrick, D. Moran and L. Radom, *J. Phys. Chem. A*, 2007, **111**, 11683–11700.
42 A. P. Scott and L. Radom, *J. Phys. Chem. A*, 1996, **100**, 16502–16513.
43 G. Rauhut and P. Pulay, *J. Phys. Chem. A*, 1995, **99**, 3093–3100.
44 M. J. Frisch, G. W. Trucks, H. B. Schlegel, G. E. Scuseria, M. A. Robb, J. R. Cheeseman, G. Scalmani, V. Barone, B. Mennucci, G. A. Petersson, H. Nakatsuji, M. Caricato, X. Li, H. P. Hratchian, A. F. Izmaylov, J. Bloino, G. Zheng, J. L. Sonnenberg, M. Hada, M. Ehara, K. Toyota, R. Fukuda, J. Hasegawa, M. Ishida, T. Nakajima, Y. Honda, O. Kitao, H. Nakai, T. Vreven, J. A. Montgomery, J. E. Peralta, F. Ogliaro, M. Bearpark, J. J. Heyd, E. Brothers, K. N. Kudin, V. N. Staroverov, R. Kobayashi, J. Normand, K. Raghavachari, A. Rendell, J. C. Burant, S. S. Iyengar, J. Tomasi, M. Cossi, N. Rega, J. M. Millam, M. Klene, J. E. Knox, J. B. Cross, V. Bakken, C. Adamo, J. Jaramillo, R. Gomperts, R. E. Stratmann, O. Yazyev, A. J. Austin, R. Cammi, C. Pomelli, J. W. Ochterski, R. L. Martin, K. Morokuma, V. G. Zakrzewski, G. A. Voth, P. Salvador, J. J. Dannenberg, S. Dapprich, A. D. Daniels, Ö. Farkas, J. B. Foresman, J. V. Ortiz, J. Cioslowski and D. J. Fox, *Gaussian, Inc.*, Wallingford CT, 2009.
45 N. Martsinovich, D. R. Jones and A. Troisi, *J. Phys. Chem. C*, 2010, **114**, 22659–22670.
46 J. P. Perdew, K. Burke and M. Ernzerhof, *Phys. Rev. Lett.*, 1996, **77**, 3865–3868.
47 R. Car and M. Parrinello, *Phys. Rev. Lett.*, 1985, **55**, 2471–2474.
48 P. Giannozzi, S. Baroni, N. Bonini, M. Calandra, R. Car, C. Cavazzoni, D. Ceresoli, G. L. Chiarotti, M. Cococcioni, I. Dabo, A. D. Corso, S. d. Gironcoli, S. Fabris, G. Fratesi, R. Gebauer, U. Gerstmann, C. Gougoussis, A. Kokalj, M. Lazzeri, L. Martin-Samos, N. Marzari, F. Mauri, R. Mazzarello, S. Paolini, A. Pasquarello, L. Paulatto, C. Sbraccia, S. Scandolo, G. Sclauzero, A. P. Seitsonen, A. Smogunov, P. Umari and R. M. Wentzcovitch, *J. Phys.: Condens. Matter*, 2009, **21**, 395502.
49 J. P. Muscat and D. M. Newns, *Prog. Surf. Sci.*, 1978, **9**, 1–43.
50 P. Persson, M. J. Lundqvist, R. Ernstorfer, W. A. Goddard and F. Willig, *J. Chem. Theory Comput.*, 2006, **2**, 441–451.
51 A. D. Khalaji, K. Fejfarova and M. Dusek, *Acta Crystallogr., Sect. E: Struct. Rep. Online*, 2011, **67**, o3508–o3509.
52 J. M. Azpiroz, E. Mosconi and F. D. Angelis, *J. Phys. Chem. C*, 2011, **115**, 25219–25226.
53 P. Persson, R. Bergström and S. Lunell, *J. Phys. Chem. B*, 2000, **104**, 10348–10351.
54 S. Manzhos, H. Segawa and K. Yamashita, *Phys. Chem. Chem. Phys.*, 2012, **14**, 1749–1755.
55 F. Labat and C. Adamo, *J. Phys. Chem. C*, 2007, **111**, 15034–15042.
56 F. De Angelis, *Chem. Phys. Lett.*, 2010, **493**, 323–327.
57 N. Martsinovich and A. Troisi, *J. Phys. Chem. C*, 2011, **115**, 11781–11792.

58 D. Rocca, R. Gebauer, F. De Angelis, M. K. Nazeeruddin and S. Baroni, *Chem. Phys. Lett.*, 2009, **475**, 49–53.
59 F. De Angelis, S. Fantacci, E. Mosconi, M. K. Nazeeruddin and M. Grätzel, *J. Phys. Chem. C*, 2011, **115**, 8825–8831.
60 F. Schiffmann, J. VandeVondele, J. r. Hutter, R. Wirz, A. Urakawa and A. Baiker, *J. Phys. Chem. C*, 2010, **114**, 8398–8404.
61 F. De Angelis, S. Fantacci, A. Selloni, M. K. Nazeeruddin and M. Grätzel, *J. Am. Chem. Soc.*, 2007, **129**, 14156–14157.
62 F. Ambrosio, N. Martsinovich and A. Troisi, *J. Phys. Chem. Lett.*, 2012, **3**, 1531–1535.
63 K. Srinivas, K. Yesudas, K. Bhanuprakash, V. J. Rao and L. Giribabu, *J. Phys. Chem. C*, 2009, **113**, 20117–20126.
64 E. Mosconi, A. Selloni and F. De Angelis, *J. Phys. Chem. C*, 2012, **116**, 5932–5940.
65 E. Ronca, M. Pastore, L. Belpassi, F. Tarantelli and F. De Angelis, *Energy Environ. Sci.*, 2013, **6**, 183–193.
66 M. Landmann, E. Rauls and W. G. Schmidt, *J. Phys.: Condens. Matter*, 2012, **24**, 195503.
67 N. Martsinovich and A. Troisi, *Energy Environ. Sci.*, 2011, **4**, 4473–4495.
68 J. P. Perdew, *Int. J. Quantum Chem.*, 1985, **28**, 497–523.
69 S. Rühle, M. Greenshtein, S. G. Chen, A. Merson, H. Pizem, C. S. Sukenik, D. Cahen and A. Zaban, *J. Phys. Chem. B*, 2005, **109**, 18907–18913.